Relationship between structure, dynamics, and mechanical properties in metallic glass-forming alloys

Y. Q. Cheng,[1,*] H. W. Sheng,[2] and E. Ma[1]
[1]*Department of Materials Science and Engineering, Johns Hopkins University, Baltimore, Maryland 21218, USA*
[2]*Department of Computational and Data Sciences, George Mason University, Fairfax, Virginia 22030, USA*
(Received 23 June 2008; published 30 July 2008)

Using Cu-Zr models, we demonstrate icosahedral ordering as a microscopic origin of the non-Arrhenius dynamical slowing down in metallic supercooled liquids. This correlation between the structural and dynamical heterogeneities underlies the evolution of the energy barrier for relaxation upon undercooling, as well as the eventual glass transition that leads to the formation of bulk metallic glasses (MGs). Our analysis of the energy barrier to plastic relaxation in MGs relates their macroscopic strength and plasticity to the local structures developed in the MGs. The structure-dynamics perspective explains not only the composition-dependent mechanical properties but also the known correlation between the strength of MGs and the glass transition temperature.

DOI: 10.1103/PhysRevB.78.014207 PACS number(s): 61.43.Dq, 61.20.Ja, 62.20.F−, 66.20.Cy

I. INTRODUCTION

The intense research into the bulk metal glasses (BMGs) has recently revealed a strong composition dependence of their mechanical properties.[1–5] As an example, in Cu_xZr_{100-x} BMGs, the yield stress (σ_y) increases markedly from 1.6 to 2.1 GPa, while the plastic strains gradually diminish with increasing Cu content from $x=46$ to 65.[5] If these were conventional crystalline alloys, to explain such composition-dependent mechanical behavior one would be looking for differences in microstructure, including the fractions and morphology of coexisting phases, their crystal structures and degree of order, and the contents and distributions of defects (such as dislocations and grain boundaries). However, the invariably amorphous BMGs have no such "microstructure" to speak of. It is therefore a major challenge to establish structure-mechanical property relationship for these glassy materials.

On a macroscopic level, the mechanical behavior can be correlated with characteristic parameters measured for the BMGs, such as the glass transition temperature,[6,7] T_g, and the elastic constants including Poisson's ratio.[8,9] However, on a more fundamental level, all these indicators and their empirical correlations also have common origin in the internal structure of the BMGs.[10] The purpose of this paper is to use molecular-dynamics (MD) simulations to explore the structural basis of the mechanical properties of BMGs, via the structure-dynamics correlations in their parent supercooled liquids, using Cu_xZr_{100-x} MGs ($x=46$ to 65) as models.[5,11]

II. MODEL SYSTEMS

Many-body interatomic interaction potentials employing the embedded atom method (EAM) formalism were developed for the Cu-Zr system using the force-matching method[12] by fitting the predetermined potential-energy landscape (PEL),[13] i.e., potential energies, atomic forces, and stress tensors of the ensembles. The PEL was first surveyed via VASP (Refs. 14–16) *ab initio* simulations of over 500 atomic configurations, typically consisting of 96–128 atoms for crystalline, liquid, and glass phases. The generated EAM parameters were further refined using a recursive method and validated against a large set of experimental and *ab initio* data. The potential development is a rather lengthy and involved process and the details will have to be reported elsewhere.[17] *NPT* ensembles ($P=0$) of five alloys ($x=46$, 50, 55, 60, and 64), containing 10 000 atoms with periodic boundary conditions, were melted and equilibrated at 2000 K for 2 ns (time step 2 fs) and cooled down to 300 K at 100 K/ns. The configurations were monitored using the Voronoi tessellation method to yield information about the atomic packing, such as the pair distribution functions (PDFs), coordination numbers (CNs), and types of coordination polyhedra.[10] The eventual MG structures were validated by comparing the x-ray diffraction and extended x-ray absorption fine structure calculated for the configurations with those measured in experiments; examples will be given elsewhere,[17] and the procedural details have been presented before for other alloys.[10]

III. COMPOSITION-DEPENDENT MG STRUCTURES

Figure 1(a) displays the molar volume (V_m) for the MG configurations. The composition dependence falls on a straight line that interpolates V_m of pure fcc Cu and hcp Zr, in agreement with experiments.[11] There is no noticeable volumetric advantage for any specific x. The local ordering, on the other hand, is found to depend strongly on x, in terms of the dominant types of Voronoi polyhedra around Cu. Among all the Cu-centered coordination polyhedra, the fractions of full icosahedra (Voronoi index $\langle 0,0,12,0\rangle$) and the distorted icosahedra $\langle 0,2,8,2\rangle$ are more than doubled at the expense of some other polyhedral types, as shown in Fig. 1(b). Since each Cu-centered icosahedron contains 13 atoms, the fraction of the total number of Cu and Zr atoms involved in the full icosahedra, $f_{\mathrm{ico}}^{\mathrm{atoms}}$, climbs to as high as 80% at $x=64$.

Figure 1(c) demonstrates the development of icosahedral ordering throughout the supercooled liquid region between the liquidus temperature, T_l, and glass transition temperature,

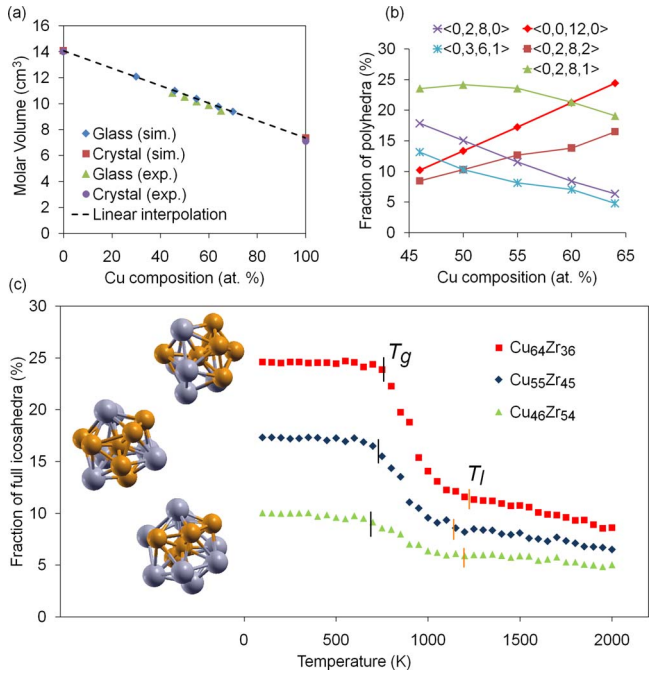

FIG. 1. (Color online) (a) Molar volume of Cu_xZr_{100-x} MGs, from MD simulations at 300 K, compared with experimental data (Ref. 11). (b) Fraction of dominant Voronoi polyhedra at various x. (c) Evolution of Cu-centered full icosahedral order with cooling for three example compositions. T_g values were determined by MD simulation and T_l taken from literature (Refs. 11, 31, and 32). Inherent structures were used to eliminate thermal fluctuation, and each data point is an average of ten inherent structures. Insets are the representative full icosahedra. Smaller (orange color online) atoms are for Cu and larger (gray color online) ones for Zr.

T_g. This ordering is more pronounced at higher x, which is consistent with Fig. 1(b). The insets display the representative Cu-centered full icosahedra motifs at various x. In the first shell of the center Cu atom, the most popular ratio of Cu to Zr increases from 4:8 at x=46 to 7:5 at x=64. This increase moves the effective atomic size ratio (first shell to center Cu) closer to that required for ideal icosahedral packing [0.902 (Refs. 10, 18, and 19)], topologically promoting the formation of full icosahedra around Cu.

This trend of composition-dependent structural ordering, i.e., $f_{\text{ico}}^{\text{atoms}}$, and the fraction of full icosahedra, f_{ico}, appears similar to the σ_y–x dependence measured by Park *et al.*[5] One is then tempted to plot a structure-property correlation, as shown in Fig. 2. However, one cannot establish a firm relationship linking the mechanical property with the underlying MG structure based merely on superficial resemblance of parallel trends or an apparent correlation. We therefore set out to uncover the physical basis, through the following steps.

IV. MODEL BASED ON POTENTIAL-ENERGY LANDSCAPE

Our first step is to examine what determines the strength (the resistance to plastic relaxation at room temperature, T_R). From the PEL perspective,[13] it is the configurational hopping

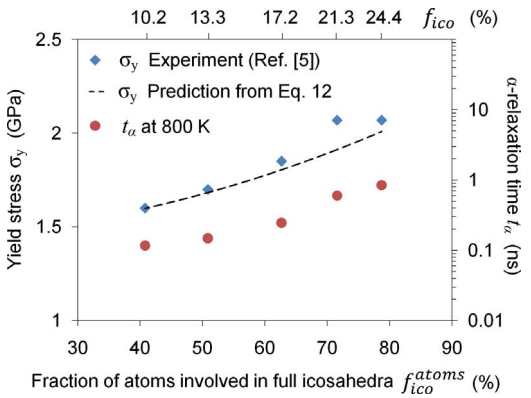

FIG. 2. (Color online) Yield stress (σ_y from Ref. 5) and α-relaxation time (t_α) correlated with structural features, $f_{\text{ico}}^{\text{atoms}}$ and f_{ico}, for the five MGs. The predicted trend (dashed line) was obtained by fitting the calculated σ_y based on Eq. (12) using simulated T_g and V_m, as well as the known σ_y for $Cu_{46}Zr_{54}$ (Ref. 5).

between different megabasins, in particular, the irreversible, or plastic, α relaxation,[7,20] that controls the rheological and mechanical properties.

Following the work of Johnson and Samwer,[7] the potential-energy density in MGs can be modeled as

$$\phi(\gamma) = \phi_{0T} \sin^2\left(\frac{\pi\gamma}{4\gamma_C}\right), \tag{1}$$

where ϕ_{0T} is the total barrier energy density for the unstressed glass at temperature T. The energy barrier is located at $2\gamma_C$, where γ_C is the critical yield strain and $4\gamma_C$ is the configurational spacing in the PEL.[7] Starting from this simple assumption, a number of physical properties of the glass can be derived. For example, the athermal critical stress, i.e., the critical shear stress at yielding without the assistance of thermal activation, is[7]

$$\tau_{C0} = \frac{\pi\phi_{0T}}{4\gamma_C}, \tag{2}$$

and the shear modulus of the unstressed MG is

$$G_{0T} = \frac{\pi^2\phi_{0T}}{8\gamma_C^2}. \tag{3}$$

A shear transformation involves N atoms, where $N \sim 100$ atoms,[7] and the average atomic volume is V_a. The potential-energy barrier for a shear transformation, W_{0T}, is then

$$W_{0T} = \phi_{0T}\zeta N V_a = (8/\pi^2) G_{0T}\gamma_C^2 \zeta N V_a, \tag{4}$$

where ζ is a correction factor arising from matrix confinement.[7] By combining Eqs. (2) and (4), we have

$$\tau_{C0} = \frac{\pi W_{0T}}{4\gamma_C \zeta N V_a}. \tag{5}$$

Again, this is the yield stress without the assistance of thermal activation. In other words, the shear transformation barrier would be completely overcome by this applied stress

alone. Note that the sampled energy landscape and barrier (W_{0T}) depend on temperature T.

Our problem deals with the strength at room temperature, T_R. We therefore examine the temperature regime of $T<T_g$. The atomic configuration has been frozen in a megabasin of the PEL, but the energy barrier of this megabasin, W_{0T}, is still changing with T. As related above in Eq. (3), the change in ϕ_{0T} is reflected by G_{0T}, which exhibits a weak dependence on T for $T<T_g$, due to the Debye-Grüneisen thermal expansion.[7,21,22] From Eq. (4), the T dependence of W_{0T} can be expressed as

$$\frac{W_{0T}}{W_{0Tg}} = \frac{G_{0T}}{G_{0Tg}}. \tag{6}$$

We know that W_{0Tg} scales with T_g via[7] (also see below)

$$W_{0Tg} = \beta T_g. \tag{7}$$

Making use of Eqs. (6) and (7), we can then rewrite Eq. (5) as

$$\tau_C = \frac{\pi \beta T_g}{4\gamma_C \zeta N V_a} \frac{G_{0T}}{G_{0Tg}}. \tag{8}$$

Johnson and Samwer[7] included the contribution of thermal activation to yielding and obtained a universal $[T/T_g]^{2/3}$ dependence,

$$\tau_{\mathrm{CT}} = \tau_C - \tau_C[\alpha(G_{0T}/G_{0Tg})]^{2/3}\left[\frac{T}{T_g}\right]^{2/3}, \tag{9}$$

where α is a constant for a given shear strain rate, and τ_{CT} is the critical shear stress at T for the stress-assisted thermally activated yielding. Substituting Eq. (8) into Eq. (9), we obtain

$$\tau_{\mathrm{CT}} = \frac{\pi}{4\gamma_C \zeta N V_a} \frac{G_{0T}}{G_{0Tg}} \beta T_g \left\{1 - [\alpha(G_{0T}/G_{0Tg})]^{2/3}\left[\frac{T}{T_g}\right]^{2/3}\right\}. \tag{10}$$

In Eq. (10), V_a scales with molar volume V_m, γ_C can be considered universal for all MGs,[7] and ζ and N are not expected to vary significantly for the Cu-Zr MGs we are studying. G_{0T}/G_{0Tg} has a rather weak temperature dependence, and the upper limit was estimated to be ~7% for Vitreloy 1 by varying T from T_g all the way to 0 K.[7]

The focus of our discussion is the T_g (or composition) dependence of strength at the fixed T_R. Equation (10) can be rewritten as

$$\tau_{\mathrm{CT}} = A\frac{T_g}{V_m}\left[1 - B\left(\frac{T}{T_g}\right)^{2/3}\right], \tag{11}$$

where A and B are approximately constants. By fitting with experimental data of resolved shear stress at yielding of 30 MGs, Johnson and Samwer[7] obtained fitting parameters in their $[T/T_g]^{2/3}$ correlation. A comparison with Eq. (11) indicates that the constant B can be approximated by their fitting parameters as $B=0.016/0.036=4/9$.[7] We finally have

$$\tau_{CT} = A\frac{T_g}{V_m}\left[1 - \frac{4}{9}\left(\frac{T}{T_g}\right)^{2/3}\right]. \tag{12}$$

This is the equation used to obtain the dashed line in Fig. 2. Using a different approach, Yang *et al.*[6] also proposed a similar scaling relation between the yield strength and T_g,

$$\sigma_y = C\frac{T_g - T}{V_m}. \tag{13}$$

Equation (12) could take the same form of Eq. (13) if B and the exponent in Eq. (11) are both taken as unity. Equation (12) is thus consistent with the empirical observation that the strength of MGs correlates with T_g.[6,23] As shown in Fig. 2, Eq. (12) adequately captures the trend in the experimental data in the BMG-forming range from $Cu_{46}Zr_{54}$ to $Cu_{64}Zr_{36}$.

V. STRUCTURE-DYNAMICS-STRENGTH CORRELATION

The next step for establishing the structure-strength relationship is then to assess how the structural development in the supercooled liquid changes the energy barrier for relaxation (toward W_{0Tg}) and controls the glass transition [the strength-controlling T_g in Eq. (12)]. To this end, we examine the relaxation dynamics in the supercooled liquid. The characteristic relaxation-time scale can be represented by α-relaxation time.[24] In the language of PEL, α relaxation corresponds to migration between neighboring megabasins (with a configurational spacing of $4\gamma_C$ in the model of Johnson and Samwer[7]). In deeply supercooled region, α relaxation usually consists of multiple β relaxations, and each β relaxation corresponds to a hopping event between contiguous basins residing in a much larger megabasin.[20,24] In terms of structure, β relaxation can be pictured as cage rattling and breaking of local clusters (e.g., 10–100 atoms) and α relaxation as collective progress of β-relaxation events throughout the sample, leading to macroscopic and irreversible atomic rearrangements. Thus in the PEL, the supercooled liquid loses its memory about the initial configuration, migrating to a neighboring but independent megabasin. For a MG former such as CuZr with (deep) undercooling α relaxations are retarded dramatically and deviate from Arrhenius behavior. Glass transition sets in when the relaxations are slowed down sufficiently to prohibit their observation or measurement on the laboratory time scale.[24] At this point a global irreversible relaxation is no longer possible for time scale available, and the liquid appears frozen.

In MD simulations, we can monitor the α-relaxation time, t_α, as a function of T (for $T>T_g$) during cooling. t_α is defined as the time when the self-intermediate scattering function (ISF) has decayed to e^{-1} of its initial value.[25] The ISF is the space Fourier transformation of the van Hove correlation function,[25]

$$F_s^a(q,t) = N_a^{-1}\left(\sum_{j=1}^{N_a} \exp\{i\vec{q}\cdot[\vec{r}_j^a(t) - \vec{r}_j^a(0)]\}\right), \tag{14}$$

where a denotes the element type and N denotes the number of atoms. $\vec{r}$ is the position of each atom. To determine t_α, the

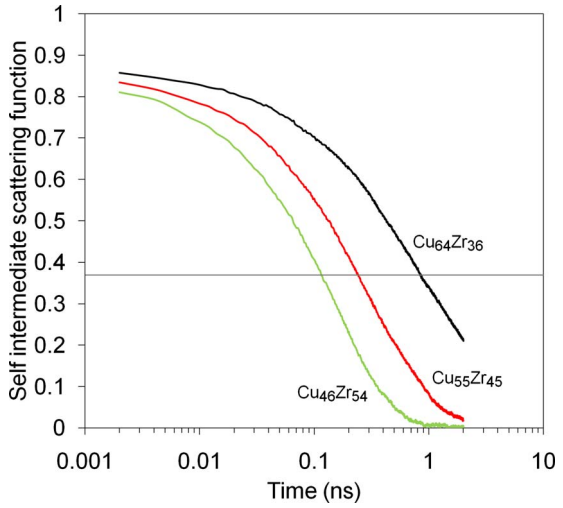

FIG. 3. (Color online) Self-intermediate scattering function (ISF) of Cu for three Cu-Zr MG-forming liquids (800 K) for characterization of the α-relaxation time. The wave vector is $q_{\max}=|\vec{q}|$, the first peak of the partial structure factors of Cu. The α-relaxation time (t_α) is defined as the time where the self-ISF has decayed to e^{-1} of its initial value (labeled by the horizontal line). Note that the α-relaxation time is a characteristic time scale of the relaxation dynamics for the whole system; in other words, if we use ISF of Zr to determine t_α, we would have similar values (Ref. 25) and the same trend.

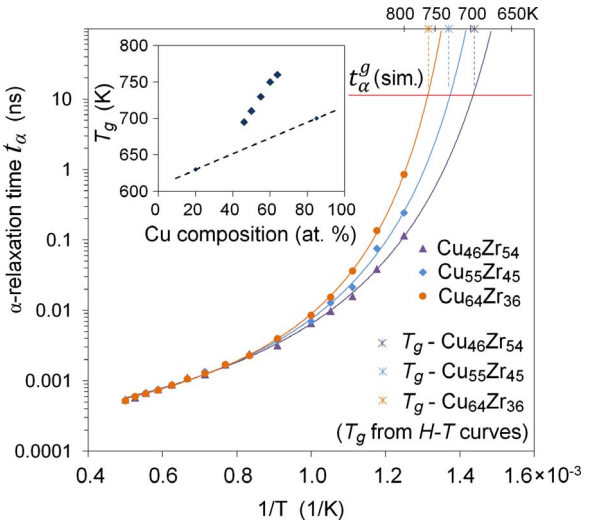

FIG. 4. (Color online) Evolution of α-relaxation time (t_α) with cooling. For clarity, only three compositions are shown. The curves are fits to the data using the VFT equation. The horizontal line corresponds to the criterion for glass transition in simulation, and T_g values determined from H-T (enthalpy T) curves are labeled with stars. The obvious composition dependence of T_g is shown in the inset, which also includes T_g for two additional simulations of $Cu_{20}Zr_{80}$ and $Cu_{85}Zr_{15}$ (smaller symbols) to demonstrate the inapplicability of interpolation assuming the rule-of-mixtures (dashed line).

wave vector q is usually fixed at $q_{\max}=|\vec{q}|$, which corresponds to the first peak of the partial structure factors of element a. As an example, we plot the ISF of three compositions at 800 K and illustrate the determination of t_α in Fig. 3. t_α scales with the viscosity[26] and directly correlates with W_{0T} via[27]

$$t_\alpha(T) = t_\alpha^\infty \exp\left[\frac{W_{0T}}{k_B T}\right], \tag{15}$$

where t_α^∞ is the high-temperature limit of relaxation time corresponding to the Planck viscosity limit for metallic systems.[27] Now Eq. (7) can be achieved by an assumption that the glass transition corresponds to a critical α-relaxation time t_α^g; thus $\ln(t_\alpha^g/t_\alpha^\infty)$ can be regarded as a constant,

$$W_{0T_g} = k_B T_g \ln(t_\alpha^g/t_\alpha^\infty) = \beta T_g. \tag{16}$$

Figure 4 is a plot showing the increasing t_α (in *logarithmic* scale) with decreasing T for our MG-forming Cu-Zr liquids, demonstrating increased W_{0T} and non-Arrhenius behavior. It is also obvious that at any given T, $t_\alpha(T)$ increases with increasing Cu content. Both the evolution of W_{0T} with T and its composition dependence at given T suggest that the barrier is elevated with increasing icosahedral ordering shown in Fig. 1(c). Due to the limited MD time scale, it is not possible to acquire t_α data very close to T_g. However, the curves can be extrapolated to T_g by fitting the data using the well-known Vogel-Fulcher-Tammann (VFT) equation.[28–30] The various Cu-Zr alloys are seen to reach the same critical t_α^g (or any given critical criterion for glass transition) at different T_g. This is, again, due to the different degrees of structural development inside. Also marked in Fig. 4 and shown in the inset are the T_g values estimated from our simulations in the enthalpy (H) versus T plots (H-T curves not shown).

Note that the T_g values obtained by H-T curves seem to project consistently to a critical t_α of ~10 ns (Fig. 4). This manifests that in the "MD-simulated laboratory", the characteristic time scale (for sample processing, observation, measurement, etc.) is indeed at a span of nanosecond. However, these T_g values are also close to experimental measurements,[11,31–33] where the characteristic time scale should be many orders of magnitude longer. These observations can be understood from the following considerations. First of all, because the MD measurement time is much shorter than in experiments, the apparent T_g in simulation would appear at a higher temperature. However, since the curves are increasingly steeper with decreasing T, a small shift of T may result in large difference of t_α, especially at T close to T_g. Therefore, even though the transition criterion t_α^g is very different for simulation and experiment, the transition temperature T_g is not going to be very different. In fact, in experiments, the observation is that T_g usually shifts no more than a few degrees when the cooling rate is changed by one order of magnitude.[32,34] On the other hand, the fast cooling rate in MD simulation limits the development of ordering such that the curves in Fig. 4 deviate from the experimental equilibrium liquids[35] in the deeply supercooled regime, pushing down T_g. The compensating effects also explain why the MD T_g values are not very different from the experimental ones. We note here once again that the MD data are not meant to reproduce experimental values for real-world MGs (as the processing conditions are different) but to provide

insight as to what controls T_g and W_{0Tg} and to capture the trend of composition-dependent properties.

In Fig. 2 we have included t_α at 800 K. The trend for t_α is obviously similar to that of σ_y. On the other hand, t_α also correlates with the structural features developed (f_{ico} and $f_{\text{ico}}^{\text{atoms}}$); also compare Fig. 1(c) and Fig. 4. These correlations establish that there is an intrinsic relation between the structure evolution, the dynamics in the supercooled liquid, and the mechanical properties of the eventual BMG.

VI. MICROSCOPIC ROLE OF ICOSAHEDRA IN CONTROLLING DYNAMICS

In Sec. V, we have demonstrated that parallel to the increase in full icosahedral packing, t_α and W_{0Tg} and T_g are all increasing with Cu content. However, to unequivocally pin down the role of the icosahedral ordering in controlling t_α and T_g (and hence σ_y, see equations above), we need one more step to directly compare the effect of the full icosahedra and other polyhedral types on relaxation dynamics. To confirm that the slow dynamics is indeed controlled by full icosahedra, we need a measure of atomic mobility, which will be used to reflect the effect of local structure on the dynamic behavior of the atoms. To this end, we first calculate the non-Gaussian parameter,[36]

$$\alpha_2(t) = \frac{3\langle r^4(t)\rangle}{5\langle r^2(t)\rangle^2} - 1, \tag{17}$$

to obtain the "maximum non-Gaussian time": t at which α_2 reaches the maximum. This time corresponds to the time when the distribution of atomic motion is the most heterogeneous, which is the late stage of cage rattling (β relaxations) or a time spot right before the liquid has performed an α relaxation. Therefore, at this time, the mean-square displacements of atoms are the most discriminating: atoms with large displacement are leading the α relaxation, while the atoms with small displacement are retarding it. We then evaluate the "propensity of motion"[37] from the atomic mean-square displacement measured for this time interval at 800 K in the supercooled liquid. 1000 simulation runs were conducted and averaged, starting from the same configuration but with independent random distribution of initial momenta (in accordance with the Maxwell-Boltzmann distribution). By averaging the mean-square displacements for the propensity of motion, we have eliminated the effect of initial momenta distribution and obtained an indicator of atomic mobility which is solely determined by the local structural environment. It was shown before that the distribution of propensity for motion is highly heterogeneous, indicating a wide range of local atomic mobility[37] (also see Fig. 5). The structural origin, however, remained unclear except in some idealized model systems such as Dzugutov liquids, where the hypothetical pair potential is designed to artificially favor icosahedral packing.[38,39]

A statistical correlation between the local structure and dynamics can be revealed as follows. As shown in Fig. 5 for $Cu_{64}Zr_{36}$, for the 5% Cu atoms with the slowest dynamics, the majority (over 70%) of them are in full icosahedra. In fact, the inset in Fig. 5 clearly indicates that the lower the

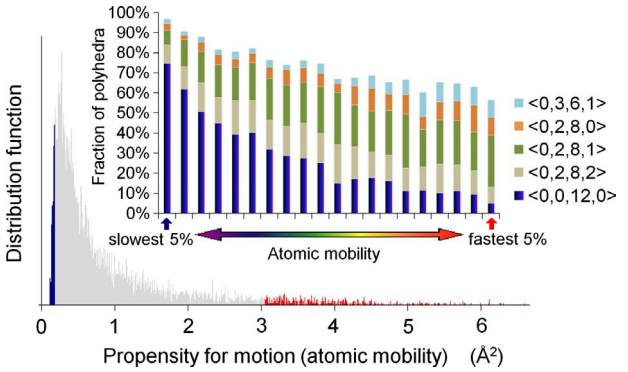

FIG. 5. (Color online) Distribution of atomic mobility (propensity for motion) of Cu in $Cu_{64}Zr_{36}$ (at 800 K). Left end (blue color online) area and right end (red color online) area mark the 5% Cu atoms with the lowest and highest mobilities, respectively. In the inset, the Cu atoms are sorted by their atomic mobility from low to high. They are divided into 20 groups, each containing 5% of the total Cu atoms. In each group, atoms are categorized by their local structural environment (Voronoi indices of the Cu-centered coordination polyhedra). The histogram shows the makeup of each of the 20 groups in terms of the percentage of each of the five most populous Voronoi polyhedra for the slowest group (left) to the fastest group (right).

mobility, the higher the concentration of full icosahedra, and vice versa. In contrast to the sensitive dependence of mobility on full icosahedra, all other types of clusters are not responsible for the slow dynamics, even though their population is significant and some of them are distorted or fragmented icosahedra and contain many fivefold bonds. A possible reason is that a full fivefold environment would be preferable and better balanced to efficiently retard the relaxation processes. The underlying mechanism, from the local PEL perspective, could be that local full icosahedral packing with complete fivefold environment corresponds to higher configurational transition barrier, which may be correlated with a deeper local minimum. For example, our preliminary calculation shows that the average configurational potential energy of Cu atoms surrounded by full icosahedra is ~0.03 eV/atom lower than those surrounded by other types of polyhedra. The elevated local configurational transition barrier, in turn, can extend the cage rattling process and delay the breakdown of the local cage that may set off α relaxation. In fact, this stabilization benefits not only the center atoms but also other atoms involved in the full icosahedra. For example, the Zr atoms involved in full icosahedra are observed to have an average atomic mobility of ~30% lower than those not belonging to any full icosahedra (see Fig. 6). Other types of polyhedra, in contrast, do not exhibit this stabilizing effect. Another interesting observation, in Fig. 5, is that the five types of the more regular polyhedra account for over 95% of the slowest atoms, while only less than 70% for the fastest atoms, indicating that there are more irregular/liquidlike clusters in the high mobility regions.

There is still one more issue to address. We know that in $Cu_{64}Zr_{36}$ full icosahedra are actually the most popular clusters [Fig. 1(b)]. They are expected to be the most comfortable local configuration for this composition. One could infer

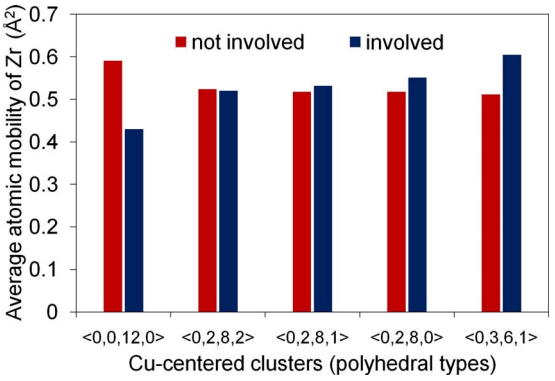

FIG. 6. (Color online) Average atomic mobility of Zr in different local environments. For each polyhedral type, Zr atoms are categorized into two groups: those that are involved in a cluster of this polyhedral type and those that are not. An average atomic mobility of Zr in each group is calculated and compared with the other group. It is seen that $\langle 0,0,12,0\rangle$ full icosahedra have stabilizing effect on the Zr involved, but other types of polyhedra do not.

that they would naturally correspond to low mobility as they would be reluctant to change. In other words, for an alloy composition where the favorable local structure is not dominated by full icosahedra, will the dominant polyhedra (a new type different from icosahedra) play the same role as the full icosahedra in $Cu_{64}Zr_{36}$? For comparison, we simulated $Cu_{20}Zr_{80}$, which is dominated by polyhedral types other than icosahedra and shows much smaller t_α. Interestingly, here there is no particular polyhedron type that can be singled out to preferentially slow down the atoms (see Fig. 7). The lack of stabilizer in $Cu_{20}Zr_{80}$ explains why its relaxation dynamics is much faster than $Cu_{64}Zr_{36}$. This is also strong proof that the development of full icosahedra in Cu-Zr is indeed directly responsible for slowing down the dynamics, effectively increasing W_{0T}, discouraging basin hopping and prolonging t_α.[20]

We note that for MG-forming liquids, although the rheology is known to depend on configurational potential energy,[27] an understanding directly connecting structural order with dynamics has not been available before. A more pronounced dynamical slowing down leads to higher T_g, see Fig. 4 (and correspondingly higher W_{0T_g}). The full icosahedra order is therefore also responsible for the increased resistance to stress-driven shear transformations (plastic relaxation events for flow) at T_R.

VII. CONCLUDING REMARKS

In summary, the atomistic models presented here, while not meant to capture absolute property values of real-world alloys, enabled us to identify full icosahedra ordering as the structural origin of the dynamical slow down that controls T_g (and W_{0T_g}), which in turn scales with the strength of the MG at T_R [see derivation leading to Eq. (12)]. The composition dependence of this development of structural and dynamical heterogeneities is responsible for the obviously composition-dependent T_g and mechanical behavior (such as strength and plasticity) observed in experiments.[5,11] T_g appears to be an easily accessible indicator of the strength of MGs,[6,23] but on a deeper level, our analysis demonstrates that it is the intrinsic structural evolution that determines macroscopic properties.

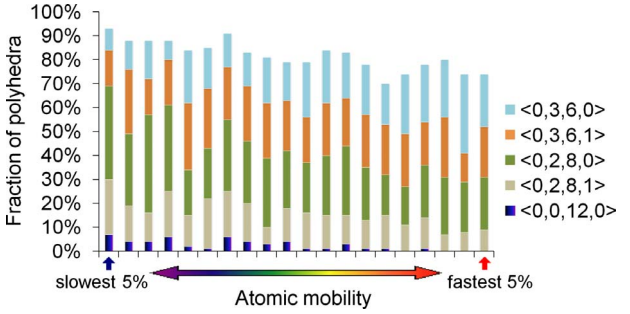

FIG. 7. (Color online) Same as the inset of Fig. 5 but for $Cu_{20}Zr_{80}$.

By "structure," we refer to information pertaining to chemical make-up and atomic bonding involved in the atomic cluster, in addition to local order. All these are interdependent effects that cannot be isolated: the enhanced full icosahedral ordering with increasing Cu content goes hand in hand with the appropriate composition ratios and bond types, which chemically, topologically, and kinetically stabilize the local icosahedral motifs. Together, these structural effects lead to the higher resistance to shear transformations and hence also reduced propensity for plasticity.[5]

Note that the experimental properties[5] and the underlying composition-dependent structure, especially the $\langle 0,0,12,0\rangle$ full icosahedral order important for slow dynamics, cannot be represented by a simple rule-of-mixtures interpolation. Simulations of Zr-rich and very Cu-rich MGs indicate reduced stability of icosahedral order and low T_g (to illustrate this point the latter is shown in the inset in Fig. 4).

ACKNOWLEDGMENTS

This work was supported by Division of Materials Sciences and Engineering, U.S. DOE-BES under Contract No. DE-FG02-03ER46056.

*cheng@jhu.edu

[1] R. D. Conner and W. L. Johnson, Scr. Mater. **55**, 645 (2006).
[2] Y. H. Liu, G. Wang, R. J. Wang, D. Q. Zhao, M. X. Pan, and W. H. Wang, Science **315**, 1385 (2007).
[3] L. Y. Chen, Z. D. Fu, G. Q. Zhang, X. P. Hao, Q. K. Jiang, X. D. Wang, Q. P. Cao, H. Franz, Y. G. Liu, H. S. Xie, S. L. Zhang, B. Y. Wang, Y. W. Zeng, and J. Z. Jiang, Phys. Rev. Lett. **100**, 075501 (2008).

[4] G. Kumar, T. Ohkubo, T. Mukai, and K. Hono, Scr. Mater. **57**, 173 (2007).
[5] K. Park, J. Jang, M. Wakeda, Y. Shibutani, and J. C. Lee, Scr. Mater. **57**, 805 (2007).
[6] B. Yang, C. T. Liu, and T. G. Nieh, Appl. Phys. Lett. **88**, 221911 (2006).
[7] W. L. Johnson and K. Samwer, Phys. Rev. Lett. **95**, 195501 (2005).
[8] J. J. Lewandowski, W. H. Wang, and A. L. Greer, Philos. Mag. Lett. **85**, 77 (2005).
[9] J. Schroers and W. L. Johnson, Phys. Rev. Lett. **93**, 255506 (2004).
[10] H. W. Sheng, W. K. Luo, F. M. Alamgir, J. M. Bai, and E. Ma, Nature (London) **439**, 419 (2006).
[11] N. Mattern, A. Schöps, U. Kühn, J. Acker, O. Khvostikova, and J. Eckert, J. Non-Cryst. Solids **354**, 1054 (2008).
[12] F. Ercolessi and J. B. Adams, Europhys. Lett. **26**, 583 (1994).
[13] F. H. Stillinger, Science **267**, 1935 (1995).
[14] G. Kresse and J. Furthmüller, Comput. Mater. Sci. **6**, 15 (1996).
[15] P. E. Blöchl, Phys. Rev. B **50**, 17953 (1994).
[16] G. Kresse and D. Joubert, Phys. Rev. B **59**, 1758 (1999).
[17] Y. Q. Cheng, E. Ma, and H. W. Sheng (unpublished).
[18] D. R. Nelson, Phys. Rev. B **28**, 5515 (1983).
[19] D. R. Nelson and F. Spaepen, Solid State Phys. **42**, 1 (1989).
[20] J. S. Harmon, M. D. Demetriou, W. L. Johnson, and K. Samwer, Phys. Rev. Lett. **99**, 135502 (2007).
[21] G. Duan, M. L. Lind, M. D. Demetriou, and W. L. Johnson, Appl. Phys. Lett. **89**, 151901 (2006).
[22] M. L. Lind, G. Duan, and W. L. Johnson, Phys. Rev. Lett. **97**, 015501 (2006).
[23] X. Q. Zhang, W. Wang, E. Ma, and J. Xu, J. Mater. Res. **20**, 2910 (2005).
[24] P. G. Debenedetti and F. H. Stillinger, Nature (London) **410**, 259 (2001).
[25] W. Kob and H. C. Andersen, Phys. Rev. E **52**, 4134 (1995).
[26] L. Larini, A. Ottochian, C. De Michele, and D. Leporini, Nat. Phys. **4**, 42 (2008).
[27] W. L. Johnson, M. D. Demetriou, J. S. Harmon, M. L. Lind, and K. Samwer, MRS Bull. **32**, 644 (2007).
[28] H. Vogel, Phys. Z. **22**, 645 (1921).
[29] G. S. Fulcher, J. Am. Ceram. Soc. **8**, 339 (1925).
[30] G. Tammann and W. Hess, Z. Anorg. Allg. Chem. **156**, 245 (1926).
[31] D. H. Xu, G. Duan, and W. L. Johnson, Phys. Rev. Lett. **92**, 245504 (2004).
[32] D. H. Xu, B. Lohwongwatana, G. Duan, W. L. Johnson, and C. Garland, Acta Mater. **52**, 2621 (2004).
[33] D. Wang, Y. Li, B. B. Sun, M. L. Sui, K. Lu, and E. Ma, Appl. Phys. Lett. **84**, 4029 (2004).
[34] M. D. Ediger, C. A. Angell, and S. R. Nagel, J. Phys. Chem. **100**, 13200 (1996).
[35] R. Busch, E. Bakke, and W. L. Johnson, Acta Mater. **46**, 4725 (1998).
[36] W. Kob and H. C. Andersen, Phys. Rev. E **51**, 4626 (1995).
[37] A. Widmer-Cooper, P. Harrowell, and H. Fynewever, Phys. Rev. Lett. **93**, 135701 (2004).
[38] M. Dzugutov, S. I. Simdyankin, and F. H. M. Zetterling, Phys. Rev. Lett. **89**, 195701 (2002).
[39] J. P. K. Doye, D. J. Wales, F. H. M. Zetterling, H. M. Fredrik, and M. Dzugutov, J. Chem. Phys. **118**, 2792 (2003).